Tailor-Made Pore Surface Engineering in Covalent Organic Frameworks: Systematic Functionalization for Performance Screening

Ning Huang,[†] Rajamani Krishna,[‡] and Donglin Jiang*,[†]

[†]Department of Materials Molecular Science, Institute for Molecular Science, National Institutes of Natural Sciences, 5-1 Higashiyama, Myodaiji, Okazaki 444-8787, Japan

[‡]Van't Hoff Institute for Molecular Sciences, University of Amsterdam, Science Park 904, 1098 XH Amsterdam, The Netherlands

S *Supporting Information*

ABSTRACT: Imine-linked covalent organic frameworks (COFs) were synthesized to bear content-tunable, accessible, and reactive ethynyl groups on the walls of one-dimensional pores. These COFs offer an ideal platform for pore-wall surface engineering aimed at anchoring diverse functional groups ranging from hydrophobic to hydrophilic units and from basic to acidic moieties with controllable loading contents. This approach enables the development of various tailor-made COFs with systematically tuned porosities and functionalities while retaining the crystallinity. We demonstrate that this strategy can be used to efficiently screen for suitable pore structures for use as CO_2 adsorbents. The pore-surface-engineered walls exhibit an enhanced affinity for CO_2, resulting in COFs that can capture and separate CO_2 with high performance.

Covalent organic frameworks (COFs) are an emerging class of crystalline porous polymers with pre-designable porous structure.[1] The ordered open channels found in two-dimensional (2D) COFs could render them able to adsorb CO_2. However, the COFs' dense layer architecture results in low porosity that has thus far restricted their potential for CO_2 adsorption.[2−7] Here, we describe the use of pore surface engineering to overcome these limitations by anchoring functional groups to the pore walls to enhance the affinity of the COFs for CO_2. This method integrates a variety of functionalities with controllable loading contents onto the pore walls, which efficiently screen for structures that are suitable for CO_2 capture.

Among various types of COFs, imine-linked COFs are stable under various conditions, making them attractive for CO_2 adsorption.[2d,f,5,6e] However, conventional imine-linked COFs usually exhibit low CO_2 capacities. The conversion of imine-linked COFs into high-performance CO_2-adsorption materials is highly desired but has yet to be fully explored.

We utilized a mesoporous imine-linked porphyrin COF with a low capacity for CO_2 adsorption as a scaffold (Scheme 1). We developed a three-component reaction system consisting of 5,10,15,20-tetrakis(p-tetraphenylamino)porphyrin and a mixture of 2,5-bis(2-propynyloxy)terephthalaldehyde (BPTA) and 2,5-dihydroxyterephthalaldehyde (DHTA) at various molar ratios ($X = [BPTA]/([BPTA] + [DHTA]) \times 100 = 0, 25, 50, 75,$ and 100) for the synthesis of four COFs with different ethynyl contents on their edges (Scheme 1, $[HC\equiv C]_X$-H_2P-COFs, $X = 25, 50, 75,$ and 100). Quantitative click reactions between the ethynyl units and azide compounds were performed to anchor the desired groups onto the pore walls (Scheme 1, Supporting Information). We synthesized 20 different COFs with pores functionalized with a variety of functional groups, including ethyl, acetate, hydroxyl, carboxylic acid, and amino groups; these groups ranged from hydrophobic to hydrophilic and from basic to acidic (Scheme 1, $[R]_X$-H_2P-COFs ($[Et]_X$-H_2P-COFs, $[MeOAc]_X$-H_2P-COFs, $[EtOH]_X$-H_2P-COFs, $[AcOH]_X$-H_2P-COFs, $[EtNH_2]_X$-H_2P-COFs)).

Infrared (IR) spectroscopy provides direct evidence for the presence of ethynyl units in $[HC\equiv C]_X$-H_2P-COFs and functionalized groups in $[R]_X$-H_2P-COFs (Figure S1).[3a] Elemental analysis revealed that the actual ethynyl and functional unit contents of the COFs were close to the calculated values (Table S1). X-ray diffraction (XRD) measurements (Figure S2) revealed that $[HC\equiv C]_X$-H_2P-COFs and H_2P-COF exhibited the same XRD pattern, thereby demonstrating that the crystal structure of H_2P-COF was retained. The pore-surface-engineered COFs also exhibited the same XRD patterns as H_2P-COF (Figure S2), indicating that the crystalline framework was retained. Scheme 1B presents the pore structures of $[HC\equiv C]_{100}$-H_2P-COF, $[Et]_{100}$-H_2P-COF, $[MeOAc]_{100}$-H_2P-COF, $[EtOH]_{100}$-H_2P-COF, $[AcOH]_{100}$-H_2P-COF, and $[EtNH_2]_{100}$-H_2P-COF. The porous structures of these COFs can be fully changed through the integration of different functional groups.

Nitrogen sorption isotherms were collected at 77 K to investigate the porosity of the COFs (Figure S3). The $[HC\equiv C]_X$-H_2P-COFs exhibited Brunauer−Emmett−Teller (BET) surface areas of 1474, 1413, 962, 683, and 462 m^2 g^{-1}, corresponding to ethynyl content (X) of 0, 25, 50, 75, and 100, respectively (Table S2). This trend indicates that the ethynyl groups occupied the pore space. As a result, the pore volume decreased from 0.75 to 0.71, 0.57, 0.42, and 0.28 cm^3 g^{-1}, respectively. Notably, these COFs contained only one type of pore in the framework (Figure S4), indicating that the ethynyl units were randomly integrated into the pore walls of [HC≡

Scheme 1. (A) Schematic of Pore Surface Engineering of Imine-Linked COFs with Various Functional Groups via Click Reactions; (B) Pore Structures of COFs with Different Functional Groups (Gray, C; Blue, N; Red, O)
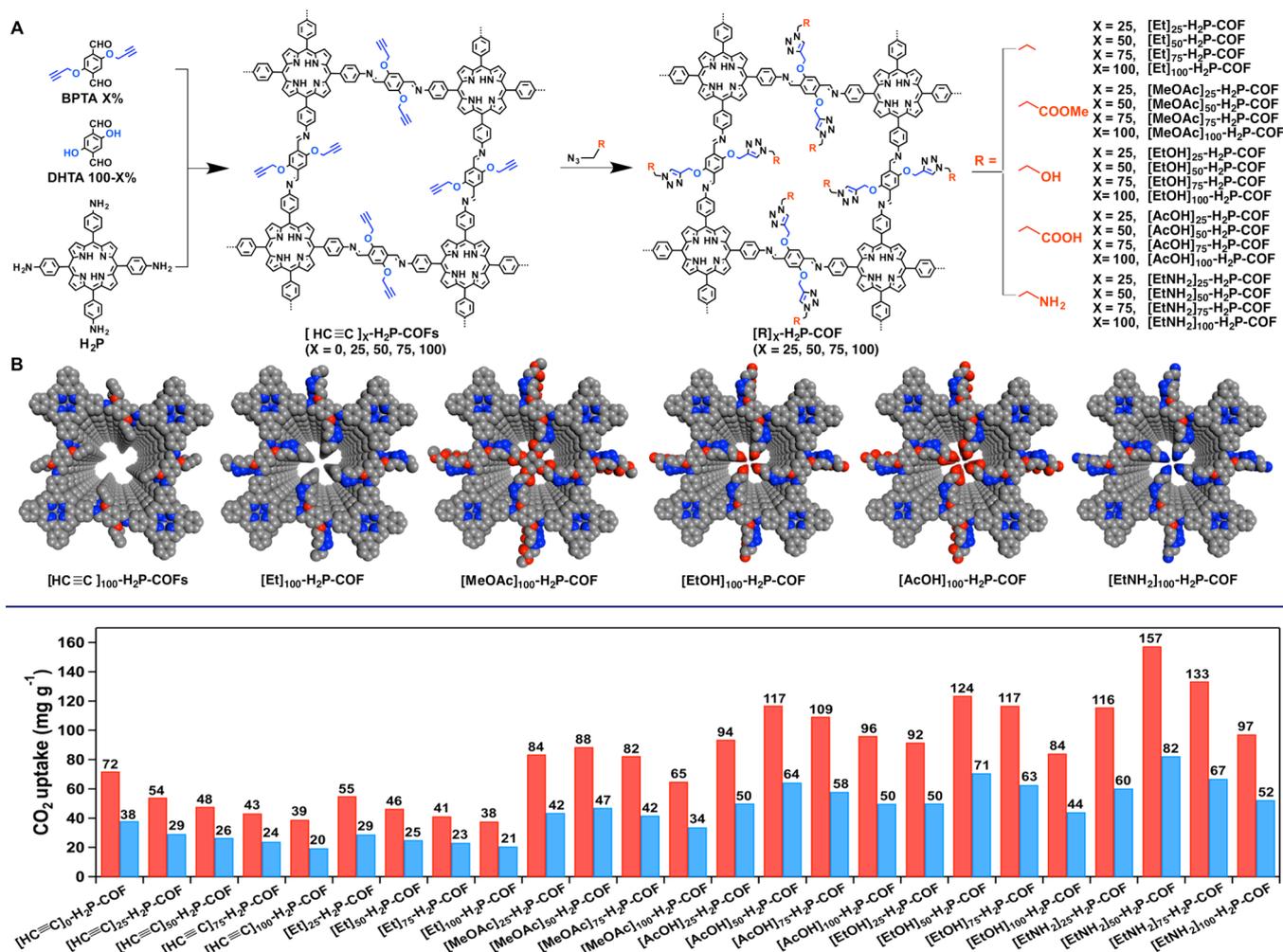
Figure 1. Carbon dioxide adsorption capacity of the COFs at 273 (red) and 298 K (blue) and 1 bar.

C]$_X$-H$_2$P-COFs (X = 25, 50, and 75). The pore size decreased from 2.5 to 2.3, 2.1, 1.9, and 1.6 nm as the X value was increased from 0 to 25, 50, 75, and 100, respectively (Table S2).

Compared to [HC≡C]$_X$-H$_2$P-COFs, the [Et]$_X$-H$_2$P-COFs with the same X value exhibited more explicit decrease in their BET surface areas, pore volumes, and pore sizes (Figure S3, Table S2). These decrease resulted from the occupation of the pores by longer chains that were integrated via pore surface engineering (Scheme 1B). For example, for [Et]$_{25}$-H$_2$P-COF, [Et]$_{50}$-H$_2$P-COF, [Et]$_{75}$-H$_2$P-COF, and [Et]$_{100}$-H$_2$P-COF, the BET surface areas were 1326, 821, 485, and 187 m^2 g^{-1}, and the pore volumes were 0.55, 0.48, 0.34, and 0.18 cm^3 g^{-1}, respectively. The pore surface engineering steadily decreased the pore size from a mesopore to supermicropores, allowing the systematic tuning of the pore sizes from 2.2 to 1.9, 1.6, and 1.5 nm. Such fine adjustments of the pore size have not been achieved via direct polycondensation. Upon pore-wall engineering with ester, hydroxyl, carboxylic acid, and amino groups, the BET surface areas, pore volumes, and pore sizes of the resulting [MeOAc]$_X$-H$_2$P-COFs, [EtOH]$_X$-H$_2$P-COFs, [AcOH]$_X$-H$_2$P-COFs, and [EtNH$_2$]$_X$-H$_2$P-COFs exhibited similar tendencies to decrease compared to those of the [Et]$_X$-H$_2$P-COFs.

The systematic integration of functional groups, in combination with a significant decrease in the pore size, makes the resulting COFs attractive for CO$_2$ adsorption (Figures S5 and S6). [HC≡C]$_X$-H$_2$P-COFs with the X values of 0, 25, 50, 75, and 100 exhibited CO$_2$ capacity of 38, 29, 26, 24, and 20 mg g^{-1}, respectively, at 298 K and 1 bar; these capacities increased to 72, 54, 48, 43, and 39 mg g^{-1} at 273 K and 1 bar (Figure 1). These results indicate that the [HC≡C]$_X$-H$_2$P-COFs are conventional COFs with low adsorption capacities. We observed that the capacity for CO$_2$ adsorption was highly dependent on the structures of the functional groups. Upon the introduction of ethyl units onto the pore walls, the resulting [Et]$_X$-H$_2$P-COFs (X = 25, 50, 75, and 100) exhibited CO$_2$ adsorption capacities similar to those of the [HC≡C]$_X$-H$_2$P-COFs under otherwise identical conditions (Figure 1). By contrast, when the functional groups were changed to ester units, the [MeOAc]$_X$-H$_2$P-COFs exhibited enhanced CO$_2$ adsorption capacities. [MeOAc]$_{50}$-H$_2$P-COF exhibites the highest capacity among the [MeOAc]$_X$-H$_2$P-COFs, with CO$_2$ adsorption capacities of 47 and 88 mg g^{-1} at 298 and 273 K, respectively (Figure 1).These values are 1.6-fold greater than those of the best-performing [Et]$_X$-H$_2$P-COFs. Notably, the introduction of carboxylic acid groups

greatly enhanced the capacity. The capacities of [AcOH]$_{25}$-H$_2$P-COF, [AcOH]$_{50}$-H$_2$P-COF, [AcOH]$_{75}$-H$_2$P-COF, and [AcOH]$_{100}$-H$_2$P-COF were 50, 64, 58, and 50 mg g^{-1} at 298 K and 94, 117, 109, and 96 mg g^{-1} at 273 K, respectively (Figure 1). The integration of hydroxyl groups similarly enhanced the adsorption. For example, [EtOH]$_{50}$-H$_2$P-COF exhibited capacities of 71 and 124 mg g^{-1} at 298 and 273 K, respectively, which are 2.3- to 2.4-fold greater than the capacities of [HC≡C]$_{25}$-H$_2$P-COF. Surprisingly, pore surface engineering with the amino groups led to an overall enhancement of CO$_2$ adsorption (Figure 1). The capacities of [EtNH$_2$]$_{25}$-H$_2$P-COF, [EtNH$_2$]$_{50}$-H$_2$P-COF, [EtNH$_2$]$_{75}$-H$_2$P-COF, and [EtNH$_2$]$_{100}$-H$_2$P-COF were 60, 82, 67, and 52 mg g^{-1} at 298 K and 116, 157, 133, and 97 mg g^{-1} at 273 K, respectively. [EtNH$_2$]$_{50}$-H$_2$P-COF exhibited the highest adsorption capacity, which was almost 3-fold greater than those of [Et]$_{50}$-H$_2$P-COF and [HC≡C]$_{50}$-H$_2$P-COF.

The dramatic change in the adsorption of CO$_2$ upon pore surface engineering is related to the interactions between functional groups and CO$_2$. The nonpolar ethynyl and ethyl groups interact weakly with CO$_2$, resulting in their poor adsorption capacity. By contrast, the polar ester units could interact with CO$_2$ via dipole interactions and thus improve the affinity of the COF for CO$_2$. The enhanced capacities of [AcOH]$_X$-H$_2$P-COFs and [EtOH]$_X$-H$_2$P-COFs resulted from the dipole and hydrogen bonding interactions of carboxylic and hydroxyl units with CO$_2$. The amino groups can form acid–base pairs with CO$_2$, leading to a significant enhancement in CO$_2$ adsorption. COFs with the same functional groups show two different tendencies with respect to CO$_2$ adsorption. The first class is the [Et]$_X$-H$_2$P-COFs, in which the pore walls have fewer interactions with CO$_2$ and thus exhibit a simple decrease in CO$_2$ adsorption capacity with X values because of their decreased surface areas and pore volumes. The second class consists of the [MeOAc]$_X$-H$_2$P-COFs, [AcOH]$_X$-H$_2$P-COFs, [EtOH]$_X$-H$_2$P-COFs, and [EtNH$_2$]$_X$-H$_2$P-COFs, which all interact strongly with CO$_2$ and exhibit maximal capacities at X = 50. This behavior is the result of a balance between the two contradictory effects of enhanced affinity and decreased porosity on adsorption. This type of perturbation indicates that precise pore surface engineering is a key component of capturing CO$_2$ with COFs.

To elucidate the nature of the CO$_2$ adsorption, we calculated the isosteric heat of adsorption (Q_{st}) from the CO$_2$ adsorption isotherm curves collected at pressures as high as 1 bar and at temperatures of 273 and 298 K (Table S2). Interestingly, the Q_{st} value increased in the order of [HC≡C]$_X$-H$_2$P-COFs ≈ [Et]$_X$-H$_2$P-COFs < [MeOAc]$_X$-H$_2$P-COFs < [AcOH]$_X$-H$_2$P-COFs < [EtOH]$_X$-H$_2$P-COFs < [EtNH$_2$]$_X$-H$_2$P-COFs (Table S2). For example, [HC≡C]$_X$-H$_2$P-COFs and [Et]$_X$-H$_2$P-COFs had Q_{st} values of 15.3−16.8 kJ mol^{-1}. The Q_{st} values of [MeOAc]$_X$-H$_2$P-COFs were higher, ranging between 16.4 and 17.8 kJ mol^{-1}. More significant enhancements in the Q_{st} values were observed for [AcOH]$_X$-H$_2$P-COFs and [EtOH]$_X$-H$_2$P-COFs; these COFs had Q_{st} values of 17.7−18.8 and 18.2−19.3 kJ mol^{-1}, respectively. [EtNH$_2$]$_X$-H$_2$P-COFs exhibited the highest Q_{st} values, which ranged from 20.4 to 20.9 kJ mol^{-1}. These results indicate that the COFs with the strongest affinity for CO$_2$ were those with pore walls that were functionalized with amino groups; those groups facilitated the adsorption of CO$_2$ and contributed to the enhanced CO$_2$ adsorption performance (ideal adsorbed solution theory (IAST) calculations of selectivity, see Figure S7).

To evaluate the gas adsorption capability of adsorbents under kinetic flowing gas conditions (CO$_2$/N$_2$ mixture containing 15% CO$_2$ and 85% N$_2$, 298 K, 100 kPa), we performed breakthrough simulations using a precise methodology established by Krishna and Long (Supporting Information, Tables S4 and S5, Figures S8 and S9).[8] These simulations accurately reflect the separation ability of a pressure-swing adsorption (PSA) process, which is an energetically efficient method for industrial-scale capture. Figure 2A shows a
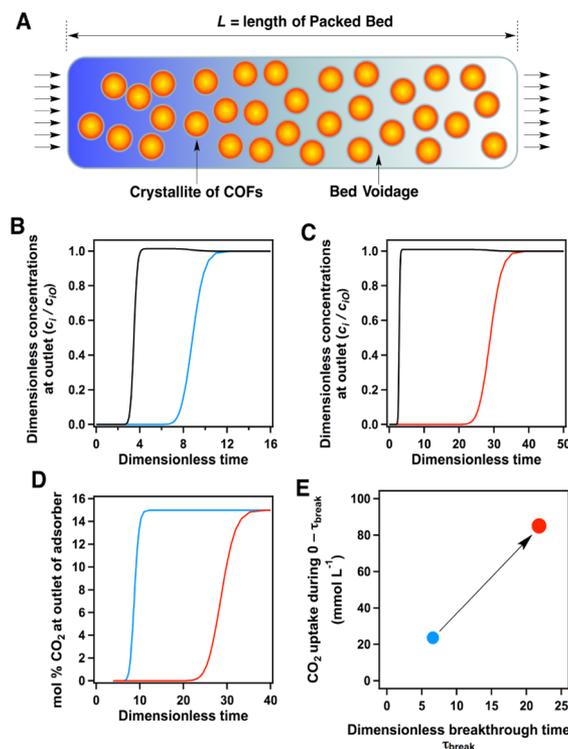
Figure 2. (A) Fixed-bed adsorber for COFs. Flue-gas breakthrough profiles of (B) [HC≡C]$_{50}$-H$_2$P-COF and (C) [EtNH$_2$]$_{50}$-H$_2$P-COF at 298 K. (D) Comparison of %CO$_2$ at the adsorber outlet at 298 K (blue curve, [HC≡C]$_{50}$-H$_2$P-COF; red curve, [EtNH$_2$]$_{50}$-H$_2$P-COF). (E) Comparison of CO$_2$ capture productivity at 298 K (blue circle, [HC≡C]$_{50}$-H$_2$P-COF; red circle, [EtNH$_2$]$_{50}$-H$_2$P-COF).

schematic of a packed-bed absorber. Figure 2B,C presents typical breakthrough curves for [HC≡C]$_{50}$-H$_2$P-COF and [EtNH$_2$]$_{50}$-H$_2$P-COF, respectively, where the x-axis is dimensionless time, τ, which is defined as the division of actual time t by the characteristic time $L\varepsilon/\mu$ (Supporting Information). [EtNH$_2$]$_{50}$-H$_2$P-COF exhibited a breakthrough time of 25, which was much longer than that of [HC≡C]$_{50}$-H$_2$P-COF (7). Figure 2D compares the breakthrough characteristics of the two COFs in terms of CO$_2$ concentration (mol%) at the absorber outlet, which is depicted as a function of dimensionless time when the operation was performed at a total pressure of 100 kPa. [EtNH$_2$]$_{50}$-H$_2$P-COF (red curve) had a breakthrough time much longer than that of [HC≡C]$_{50}$-H$_2$P-COF (blue curve). Longer breakthrough times are desirable for greater CO$_2$ capture. For a quantitative evaluation, we arbitrarily chose the required outlet gas purity as <0.05 mol % CO$_2$. Using this purity specification, we determined the breakthrough times, τ_{break}, for the COFs. Based on the material balance on the absorber, we determined the amount of CO$_2$ captured during the time interval 0−τ_{break}. Figure 2E shows the

plot of the number of millimoles of CO_2 capture per liter of adsorbent during the time interval $0 - \tau_{break}$ against the τ_{break}. Notably, $[EtNH_2]_{50}$-H_2P-COF (red circle) exhibited superior CO_2 productivity (90 mmol L^{-1}) compared to $[HC\equiv C]_{50}$-H_2P-COF (blue circle; 21 mmol L^{-1}).

COFs with highly functionalized pore wall structures are difficult to obtain via direct polycondensation reactions. The systematic pore surface engineering of COFs enables the tailor-made covalent docking of a variety of different functional groups with controlled loading contents to the pore walls. The surface engineering of the pore walls profoundly affects the surface area, pore size, pore volume, and pore environment. As demonstrated for CO_2 adsorption, pore surface engineering is a high throughput and efficient method for achieving both enhanced adsorption capacities and improved separation capabilities. Notably, this approach is not limited to the present COF and is widely applicable to many other previously reported COFs. We envisage that pore surface engineering might be a general strategy for screening for COF materials that satisfy the multiple requirements of CO_2 capture in industrial-level flow-gas applications.

■ ASSOCIATED CONTENT

ⓢ Supporting Information

Materials and method, simulations, Tables S1– S5, and Figures S1–S9. The Supporting Information is available free of charge on the ACS Publications website at DOI: 10.1021/jacs.5b04300.

■ AUTHOR INFORMATION

Corresponding Author

*jiang@ims.ac.jp

Notes

The authors declare no competing financial interest.

■ ACKNOWLEDGMENTS

■ REFERENCES

(1) (a) Côté, A. P.; Benin, A. I.; Ockwig, N. W.; O' Keeffe, M.; Matzger, A. J.; Yaghi, O. M. *Science* **2005**, *310*, 1166. (b) Wan, S.; Guo, J.; Kim, J.; Ihee, H.; Jiang, D. *Angew. Chem., Int. Ed.* **2009**, *48*, 5439. (c) Doonan, C. J.; Tranchemontagne, D. J.; Glover, T. G.; Hunt, J. H.; Yaghi, O. M. *Nat. Chem.* **2010**, *2*, 235. (d) DeBlase, C. R.; Silberstein, K. E.; Truong, T.-T.; Abruña, H. D.; Dichtel, W. R. *J. Am. Chem. Soc.* **2013**, *135*, 16821. (e) Bunck, D. N.; Dichtel, W. R. *Angew. Chem., Int. Ed.* **2012**, *51*, 1885. (f) Calik, M.; Auras, F.; Salonen, L. M.; Bader, K.; Grill, I.; Handloser, M.; Medina, D. D.; Dogru, M.; Löbermann, F.; Trauner, D.; Hartschuh, A.; Bein, T. *J. Am. Chem. Soc.* **2014**, *136*, 17802. (g) Ding, S. Y.; Wang, W. *Chem. Soc. Rev.* **2013**, *42*, 548.

(2) (a) Zeng, Y.; Zou, R.; Luo, Z.; Zhang, H.; Yao, X.; Ma, X.; Zou, R.; Zhao, Y. *J. Am. Chem. Soc.* **2015**, *137*, 1020. (b) Medina, D. D.; Rotter, J. M.; Hu, Y.; Dogru, M.; Werner, V.; Auras, F.; Markiewicz, J. T.; Knochel, P.; Bein, T. *J. Am. Chem. Soc.* **2015**, *137*, 1016. (c) Zhou, T.; Xu, S.; Wen, Q.; Pang, Z.; Zhao, X. *J. Am. Chem. Soc.* **2014**, *136*, 15885. (d) Kandambeth, S.; Shinde, D. B.; Panda, M. K.; Lukose, B.; Heine, T.; Banerjee, R. *Angew. Chem., Int. Ed.* **2013**, *52*, 13052. (e) Lanni, L. M.; Tilford, R. W.; Bharathy, M.; Lavigne, J. J. *J. Am. Chem. Soc.* **2011**, *133*, 13975. (f) Uribe-Romo, F. J.; Hunt, J. R.; Furukawa, H.; Klöck, C.; O'Keeffe, M.; Yaghi, O. M. *J. Am. Chem. Soc.* **2009**, *131*, 4570.

(3) (a) Chen, X.; Addicoat, M.; Jin, E.; Zhai, L.; Xu, H.; Huang, N.; Guo, Z.; Liu, L.; Irle, S.; Jiang, D. *J. Am. Chem. Soc.* **2015**, *137*, 3241.

(b) Feng, X.; Ding, X.; Jiang, D. *Chem. Soc. Rev.* **2012**, *41*, 6010. (c) Furukawa, H.; Yaghi, O. M. *J. Am. Chem. Soc.* **2009**, *131*, 8875.

(4) (a) Kuhn, P.; Antonietti, M.; Thomas, A. *Angew. Chem., Int. Ed.* **2008**, *47*, 3450. (b) Wang, X.; Maeda, K.; Thomas, A.; Takanabe, K.; Xin, G.; Carlsson, J. M.; Domen, K.; Antonietti, M. *Nat. Mater.* **2008**, *8*, 76. (c) Li, Z.; Feng, X.; Zou, Y.; Zhang, Y.; Xia, H.; Liu, X.; Mu, Y. *Chem. Commun.* **2014**, *50*, 13825. (d) Liu, X.; Guan, C.; Ding, S.; Wang, W.; Yan, H.; Wang, D.; Wan, L. *J. Am. Chem. Soc.* **2013**, *135*, 10470. (e) Nagai, A.; Guo, Z.; Feng, X.; Jin, S.; Chen, X.; Ding, X.; Jiang, D. *Nat. Commun.* **2011**, *2*, 536. (f) Chen, L.; Furukawa, K.; Gao, J.; Nagai, A.; Nakamura, T.; Dong, Y.; Jiang, D. *J. Am. Chem. Soc.* **2014**, *136*, 9806.

(5) (a) Huang, N.; Chen, X.; Krishna, R.; Jiang, D. *Angew. Chem., Int. Ed.* **2015**, *54*, 2986. (b) Xu, H.; Chen, X.; Gao, J.; Lin, J.; Addicoat, M.; Irle, S.; Jiang, D. *Chem. Commun.* **2014**, *50*, 1292.

(6) (a) Spitler, E. L.; Dichtel, W. R. *Nat. Chem.* **2010**, *2*, 672. (b) Colson, J. W.; Woll, A. R.; Mukherjee, A.; Levendorf, M. P.; Spitler, E. L.; Shields, V. B.; Spencer, M. G.; Park, J.; Dichtel, W. R. *Science* **2011**, *332*, 228. (c) Stegbauer, L.; Schwinghammer, K.; Lotsch, B. V. *Chem. Sci.* **2014**, *5*, 2789. (d) Fang, Q.; Zhuang, Z.; Gu, S.; Kaspar, R. B.; Zheng, J.; Wang, J.; Qiu, S.; Yan, Y. *Nat. Commun.* **2014**, *5*, 4503. (e) Rabbani, M. G.; Sekizkardes, A. K.; Kahveci, Z.; Reich, T. E.; Ding, R.; El-Kaderi, H. M. *Chem.—Eur. J.* **2013**, *19*, 3324.

(7) (a) Ding, S. Y.; Gao, J.; Wang, Q.; Zhang, Y.; Song, W.; Su, C.; Wang, W. *J. Am. Chem. Soc.* **2011**, *133*, 19816. (b) Wu, D.; Xu, F.; Sun, B.; Fu, R.; He, H.; Matyjaszewski, K. *Chem. Rev.* **2012**, *112*, 3959. (c) Wu, D.; Li, Z.; Zhong, M.; Kowalewski, T.; Matyjaszewski, K. *Angew. Chem., Int. Ed.* **2014**, *53*, 3957.

(8) (a) Krishna, R.; Long, J. R. *J. Phys. Chem. C* **2011**, *115*, 12941. (b) Mason, J. A.; Sumida, K.; Herm, Z. R.; Krishna, R.; Long, J. R. *Energy Environ. Sci.* **2011**, *4*, 3030.